2007.8.1 (Wed.)
Hiroyuki Morimoto (for D1)

Detection/Observation Methods of Short-Lived/Single Molecules

—Toward Watching "Living Molecules"—

Contents

I. Introduction

Spectroscopic methods are useful to understand detail of chemical reactions in organic chemistry. However, conventional spectroscopic methods such as NMR, IR, X-ray, etc. are difficult to apply for detection of short-lived intermediates and observation of single molecules because they usually require a sufficient accumulation time and a large number of molecules to obtain clear spectral data. Today I will introduce different spectroscopic methods which may give us a chance to overcome these limitations.

1.1 Limitations of Conventional Spectroscopic Methods

• Time resolution is usually not enough to detect short-lived intermediates.
–> It is impossible to observe rapid change of molecules (bond dissociation/formation, transition state, etc.).

• A large number of molecules is required to observe signals with sufficient S/N ratio.
–> The observed data are only an avarage of large ensembles of different molecules.

1.2 Methods to Overcome the Limitaions

• A way to overcome the time resolution problem is to use very short laser pulses to excite and detect molecules. This method, so called as femtosecond spectroscopy, allows us to understand the change in very fast chemical reactions. –> Chapter 2

• We can expect to detect single molecules using microscopic methods with high (atomic level) resolution. TEM (transmission electron microscopy) is a method which can distinguish molecules at an atomic level. This methodology makes it possible to watch each single organic molecule with sufficient spatial resolution. –> Chapter 3

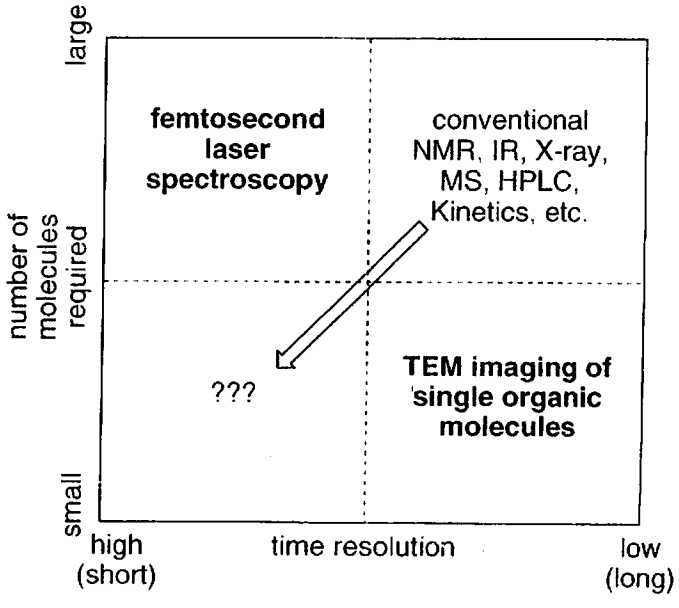

Figure 1. Classification of Methods to Observe Chemical Reactions.

2. Femtosecond Laser Spectroscopy (FLS)

2.1 Background of FLS

2.1.1 Laser (light amplification of stimulated emission of radiation)

- Laser is a form of light that is amplified in a cavity through stimulated emission process.
- Laser has the following characteristics:

1) high coherence: waves of laser are highly matched with each other.
2) single color: band width of laser is narrow.
3) pulse shaping possible: shape of laser can be modified by several optical techniques to generate femtosecond-order short pulses.

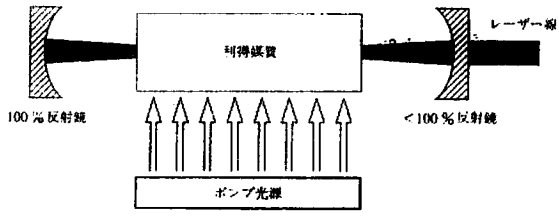

図 15·9 レーザー内部の図．利得媒質を 2 枚の鏡の間に置く．これらの部品を配列した系をレーザー空洞という．ポンプ光源が，利得媒質を構成する原子，分子，イオンを励起する．励起状態の原子から放出される輻射線を利得媒質の中で鏡を使って往復させる．一方の鏡は反射率が 100 % より小さいから，光は空洞から逃げることができる．この出力光がレーザー線である．

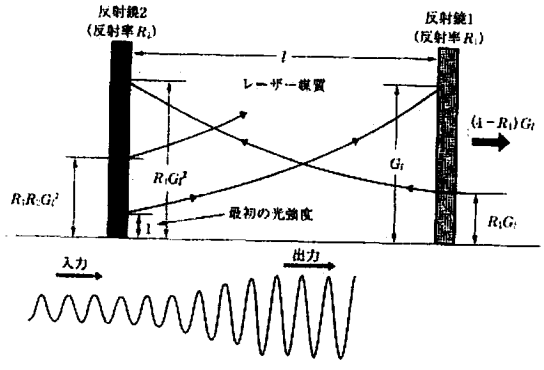

図 3·4 共振器中の光増幅の概念図

2.1.2 Pump-Probe Method—Concept of Femtosecond Spectroscopy—

- Femtosecond laser pulses are separated by beam splitter to pump and probe pulses.
- Pump pulses stimulate *reactants* to photoactivated state, which are converted to products through potential surface.
- Probe pulses excite *products* which emits fluorescence.
- Length of the probe light pathway is adjustable to control timing of arraival of the probe light (delay time).
- Obtained intensity data of fluorescence are accumulated as a function of delay time to give a graph which displays formation of products in femtosecond time scale.

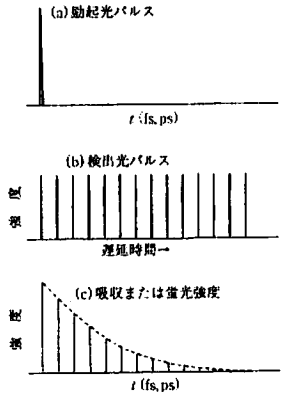

図 4·7 ポンプ・プローブ分光における励起パルスと検出パルスとの遅延時間の概念図

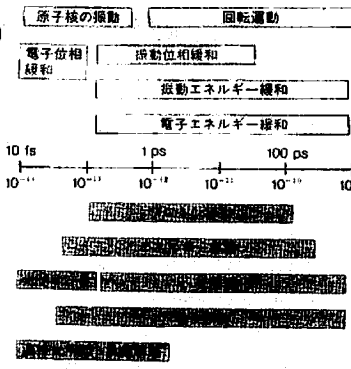

図 1 分子における種々の超高速過程．

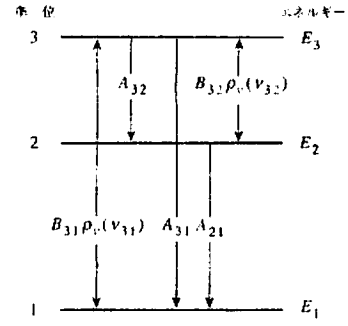

図 15·8 3 準位系のエネルギー図．振動数が $h\nu_{31} = E_3 - E_1$ のポンプ光が基底状態(状態 1)から状態 3 へ原子を励起する．この励起状態は，占有が始まると，自然放出によって状態 2 または 1 へ緩和するか，または誘導放出によって基底状態へ戻る．自然放出によって状態 2 へ緩和する励起原子は状態 1 へ戻る自然放出も起こす．エネルギーが $h\nu_{21} = E_2 - E_1$ の光が系に入射すると励起状態 3 と励起状態 2 の間で，吸収や誘導放出を起こすことができる．

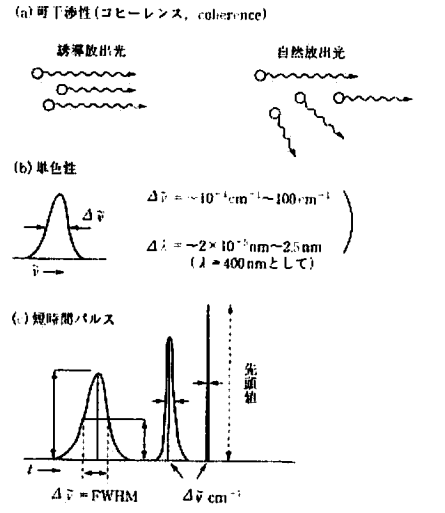

図 3·5 レーザー光の一般的性質の概念図
(a) 可干渉性，(b) 単色性（バンド幅 $\Delta\tilde{\nu}$ cm^{-1} および $\Delta\lambda$ nm），(c) レーザーパルスの時間幅，FWHM ($\Delta\tilde{\nu}$ cm^{-1}) と先頭値（ピークパワー）
ただし，パルスレーザーのバンド幅は，不確定性原理および技術的問題によりフェムト秒パルスでは $\Delta\tilde{\nu}$ = 数 100 cm^{-1}，$\Delta\lambda$ = 数 10 nm となる．

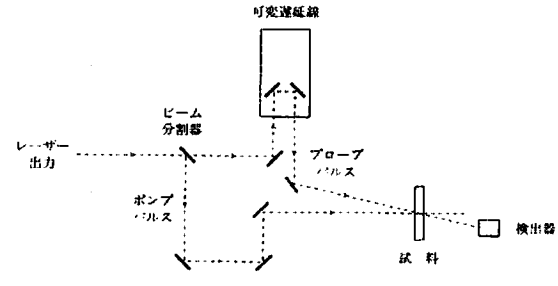

図 15·16 時間分解レーザー実験を行うために設計した装置の説明図．ビーム分割器を使ってレーザーパルスをポンプパルスとプローブパルスの二つに分割する．その二つの経路は試料内で交差する．ポンプパルスは試料に光化学過程を開始させ，プローブパルスはポンプパルスに応答して試料がどんな変化をするかを記録するのに用いる．この二つのパルスの経路長を変えると，ポンプパルスとプローブパルスが試料に到達する相対時間に影響を与える．このようにして，ポンプパルスによる励起に続いて，試料の様子が時間の関数として観測できる．

2.2 Photolysis of ICN—Proof of Concept—

2.2.1 Reaction Scheme

References: Zewail, A. H.; et al. *J. Chem. Phys.* **1987**, *87*, 2395; *Science*, **1988**, *241*, 1200; *J. Chem. Phys.* **1988**, *89*, 6113; *J. Chem. Phys.* **1988**, *89*, 6128.

$$\text{I–CN} \xrightarrow[t=0]{h\upsilon_1} [\text{I–CN}]^* \longrightarrow [\text{I}\cdots\text{CN}]^{\ddagger *} \longrightarrow \text{I}^\bullet + {}^\bullet\text{CN} \xrightarrow[t=t_n]{h\upsilon_2} [{}^\bullet\text{CN}]^{\ddagger} \xrightarrow{-h\upsilon_3} {}^\bullet\text{CN}$$

fluorescence

pump pulse (60 fs range)
$\lambda_1 = 306$ nm

probe pulse (60 fs range)
$\lambda_2 = 388.9$–390.5 nm

2.2.2 Results and Discussion

(1) Detection of •CN by 388.9 nm Probe Pulse

- Pump pulse (306 nm) excites ground state ICN to the excited potential surface, which forms a wave packet.
- The wave packet then undergoes dissociation process through the potential surface to give I• and •CN radicals.
- •CN formed was probed by delayed 388.9 nm pulses at the right side of the potential.
- Delay time of the formation of •CN was determined by signal intensities obtained from the probe pulses to be $\tau_{1/2}$ = 205±30 fs. This means this photolysis reaction completed within ~200 fs.

(2) Detection of [I- - -CN]‡* transient by 390.5 nm Probe Pulse

- Based on the structure of potential surface, excitation of [I- - - CN]‡* transient using red-side wave length probe pulse rather than 388.9 nm is possible.
- 390.5 nm probe pulse was selected to observe the transient structure, which resulted in the detection of increase and decrease of the fluorescence.
- The results indicates that we can observe not only the final products such as •CN but also detect transient intermediates [I- - -CN]‡* (so called "transition stete").
- Based on the calculation, transition state of this reaction was estimated as ≤ 50 fs.

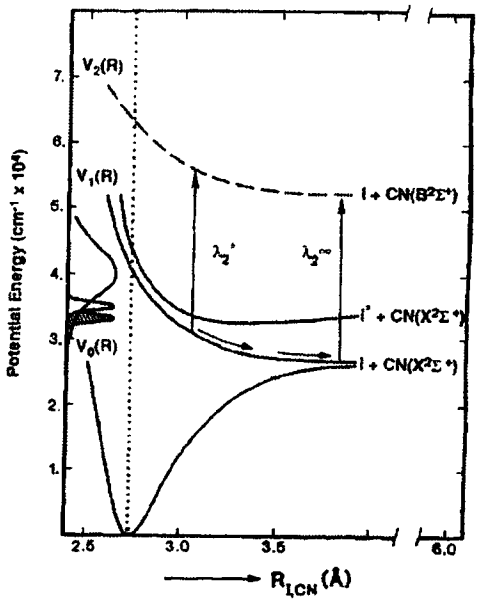

FIG. 1. Schematic of FTS and the potential energy surfaces of ICN. The pump pulse causes a vertical transition from V_0 to V_1, and the subsequent motion on this surface is indicated. The transition state is probed by λ_2^*, or the final state by λ_2^∞, which are shown by the respective arrows from V_1 to V_2. The absorption spectrum of ICN and the pump energies used are sketched on the left. Note that the difference between λ_2^* and λ_2^∞ is not to scale, and that the van der Waals wells are not shown.

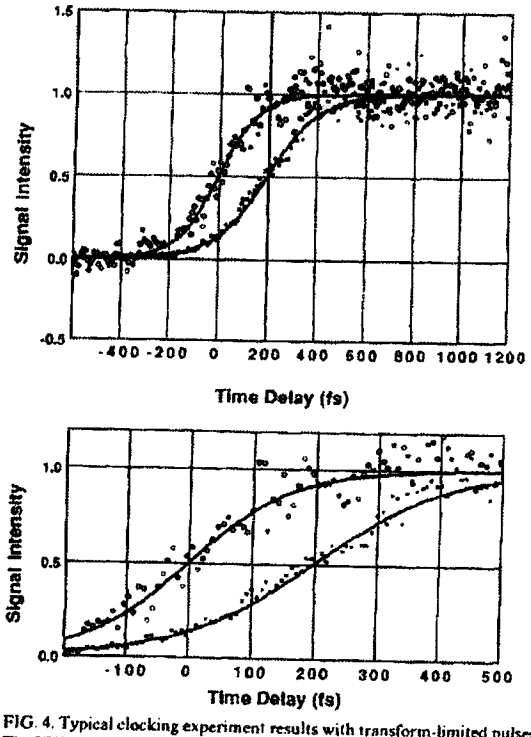

FIG. 4. Typical clocking experiment results with transform-limited pulses. The ICN transient (solid squares) in this case shows an observed delay of $\tau_{1/2} = 205 \pm 30$ fs from the DEA transient (open circles). The lines are fits to the data. The figure at the bottom shows an expanded scale near $\tau = 0$.

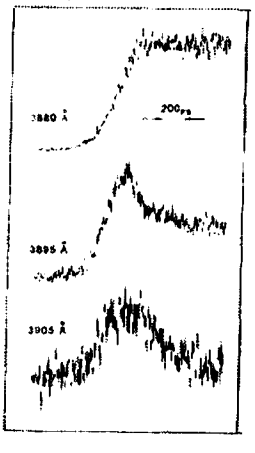

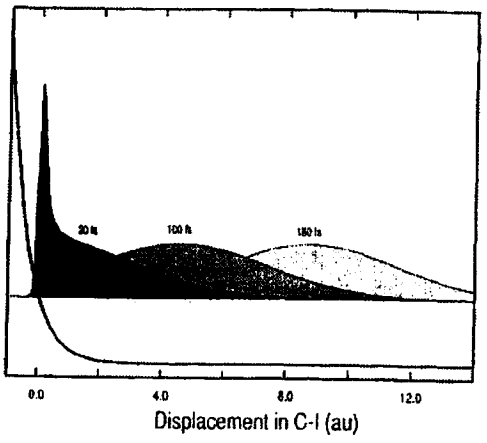

FIG. 16. Wave packet dynamics on an ICN-like PES. The figure shows the evolution of the packet on the first excited state (V_1) for a pump pulse at $\lambda_1 = 306$ nm with (a) a delta-function pulse, and (b) a 125 fs pulse. Reproduced from Ref. 31.

FIG. 1. (Right) Schematic for femtosecond probing of the transition state using a pump–probe (t, λ tuning) method. The PES are drawn to indicate the different probe wavelengths at "free" and "perturbed" CN transitions. The band on the vertical axis is the absorption spectrum (Ref. 18), and the profile of our pulse (shaded). The difference in $\lambda(R^*)$ and $\lambda(R_\infty)$ is not to scale, and the vdW wells are not shown. Note $\lambda(R^*)$ spans the different ranges of R (see the text). (Left) Femtosecond transients at the different probe wavelengths indicated. The time scale is also displayed. More detailed analysis (see Ref. 19) will be given later (Ref. 13). The experimental conditions are given in text, and these transients (each displayed on a different scale) were obtained under identical conditions except for tuning of the wavelength. The coherence time and autocorrelation traces were obtained after each scan.

2.3 Detection of Intermediates in Norrish Type-I Reaction

References: Zewail, A. H.; et al. *Science* **1994**, *266*, 1359; *Chem. Phys. Lett.* **1999**, *303*, 249; *CHEMPHYSCHEM* **2002**, *3*, 57; *CHEMPHYSCHEM* **2002**, *3*, 79.

2.3.1 Reaction Scheme

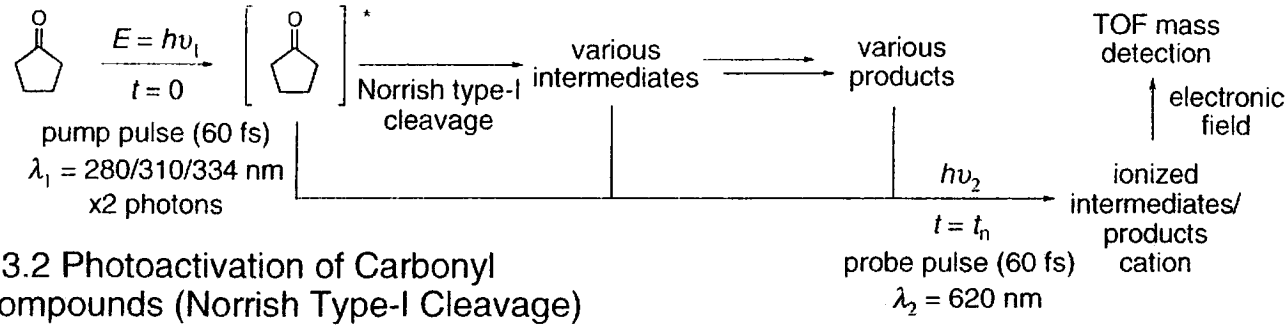

2.3.2 Photoactivation of Carbonyl Compounds (Norrish Type-I Cleavage)

- Excitation of carbonyl compounds via n-π* transition (usually ~300 nm) and subsequent cleavage of C–C bond adjacent to the carbonyl group is called for Norrish type I cleavage reaction.
- In this experiment, strong pump pulses at 280–334 nm x2 photons (equivalent to exitation at ~150 nm) were used to generate photoactivated intermediates at higher excitation state due to clean (~90% yield), instant (100–200 fs) decarbonylation and formation of various intermediates (the lowest n-π* excitation states have lifetimes of nanoseconds order and the yields vary with energy).

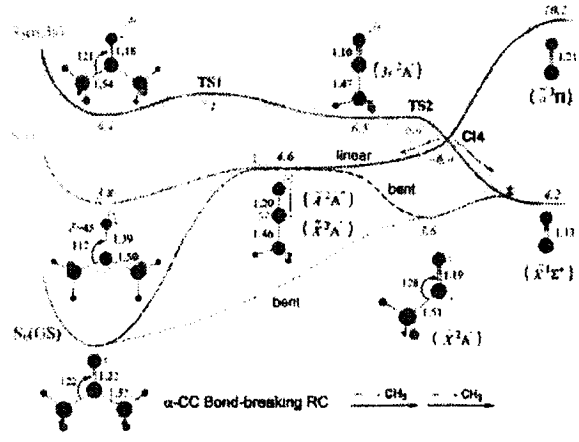

Figure 24. Schematic PES along the first and the second α-CC bond-breaking reaction coordinate for the S_0(GS), $S_1(n,\pi^*)$, and $S_2(n,3s)$ states. Both nuclear and electronic structures of the central stationary points are shown and the corresponding energies (eV) relative to the acetone S_0 minimum are given.

2.3.3 Product Detection by (Multi-) Photon Ionization–TOF Mass Combination

- Probe pulse laser is used to ionize intermediates and products.
- Ionized intermediates and products are accelerated under electronic field and detected by TOF (time-of-flight) mass apparatus.
- This method has the following advantages over the fluorescence measurement used in section 2.2: 1) molecules having no fluorescence can be detected; 2) all the molecules with different mass weights can be distinguished and detected at once; 3) selective ionization of fragments/intermediates will be possible by changing strength of the ionization conditions.

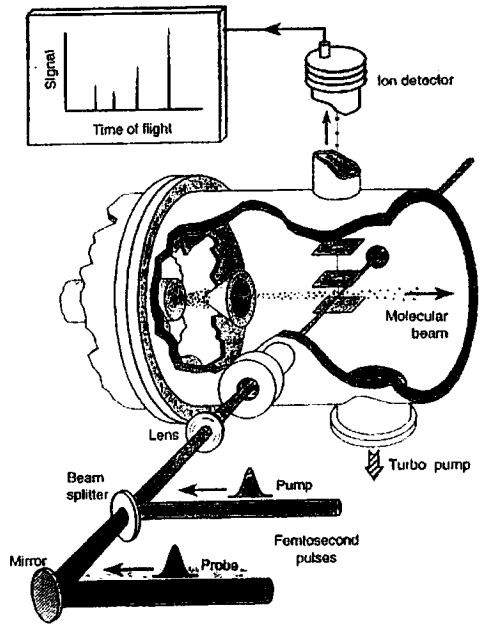

Fig. 2. The femtosecond molecular beam apparatus illustrating the mass selection and the overlap of the three beams. The femtosecond pump and probe pulses, delayed in time with respect to one another, are combined collinearly before being focused onto the molecular beam. The ions produced in the interaction region are detected in a time-of-flight mass spectrometer which can distinguish between different masses.

2.3.4 Results and Discussion

(1) Detection of Intermediates

- At delay time −100 fs (when probe pulse was arrived faster than pump pulse), no TOF mass signal was observed. This shows no ionization occurred with the probe pulse without exitation of cyclopentanone (ground state molecules can be ignored in the following mass spectra).
- At delay time 0 fs, only the parent cyclopentanone was observed at 84 amu. This indicates there is no fragmentation during probe pulse ionization process and TOF mass conditions. Therefore the mass spectra directly correlates with the state of intermediates.
- Fragment ion peaks were observed at 28, 41, 55 and 56 amus. Peaks at 28 and 41 amus would be ethylene cation radical and allyl cation signals, respectively, which were probably resulted from fragmentation of the intermediates.

(2) Time Delay Experiments

- Life time of intermediates was determined by time delay experiments similar to section 2.2.
- At first the parent ion signal increased and diradical signals followed. The parent ion signal disappeared within 700 fs whereas the other signals persisted for over 1000 fs.

(3) Investigation of Fragmentation Pathway

- Based on the MS peaks of cyclopentanone and cyclopentanone-d_4 at <50 fs delay, the major fragmentation pathway was intramolecular hydrogen rearrangement followed by C–C bond fragmentation to give the acyl radical (*m/z* 55).
- Tetramethylene diradical species were minor whereas acyl diradical species were major based on comparison of MS peak intensicties of cyclopentanone-d_4 (*m/z* 58 vs. 60).

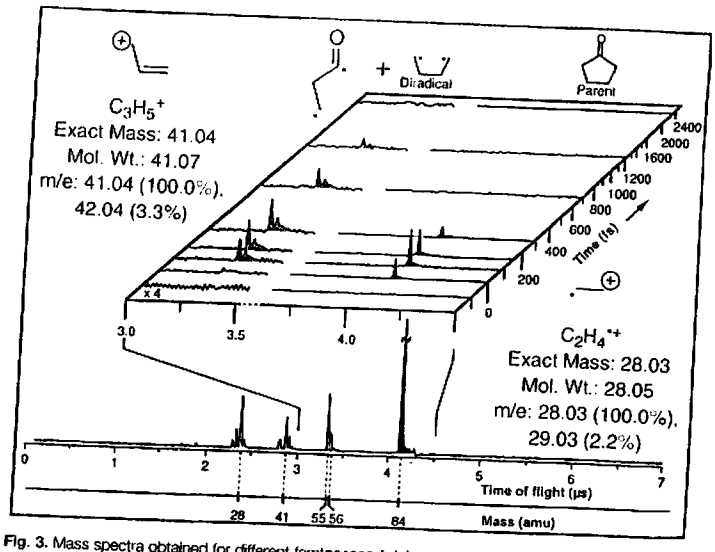

Fig. 3. Mass spectra obtained for different femtosecond delay times between the pump and probe laser pulses. The parent molecule, here cyclopentanone (84 amu), appears at zero time delay and subsequently decays. In contrast, the tetramethylene diradical intermediate (56 amu) appears later, growing in and peaking at ~300 fs, and then decays very slowly (τ_2 = 700 fs); see text. The masses at 28 and 41 amu are due to ion fragmentation and their studies will be reported elsewhere.

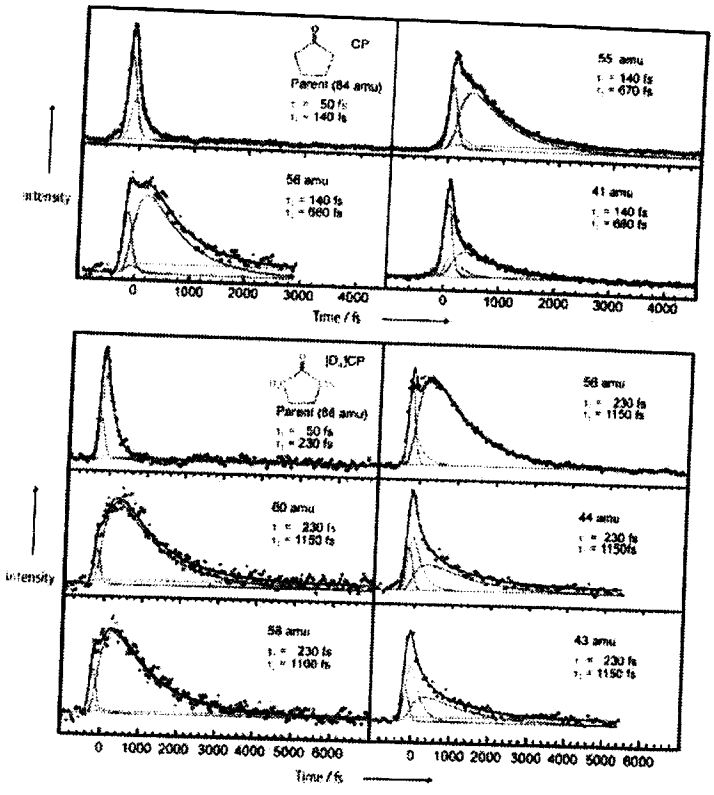

Figure 9. Transients for the parent and fragment species of CP and $[D_4]$CP. Color coding is the same as in Figure 3. An intermediate intensity of the probe was used (~15 μJ) giving a reasonable signal-to-noise ratio for the less abundant species. Note the pronounced spike-like contribution from fragmentation of the parent ion.

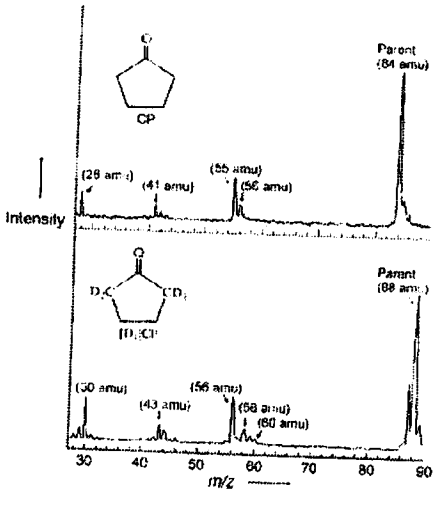

Figure 12. Multiphoton ionization mass spectra of CP and $[D_4]$CP recorded at a time delay of less than 50 fs.

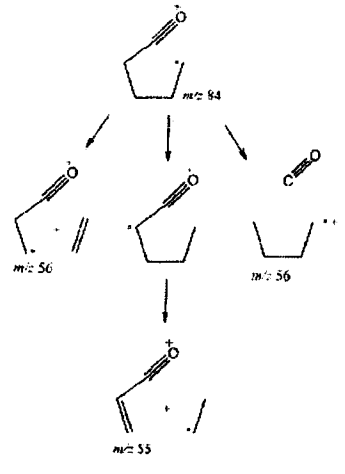

Scheme 1. Mechanism for the decomposition of CP$^{\cdot+}$.

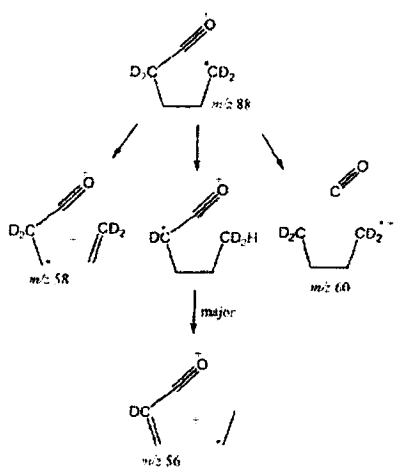

Scheme 2. Mechanism for the decomposition of $[D_4]$CP$^{\cdot+}$.

3. TEM Imaging of Single Organic Molecules

3.1 Background of TEM Imaging

3.1.1 TEM (Transmission Electron Microscope)

- TEM is a microscope using high voltage (~100–300 kV) electron beam as "light" to observe materials with atomic order resolution (~0.1 nm).
- To observe materials by TEM, the materials have to be 1) stable under high vaccuum conditions (~10^{-6} Pa); 2) tolerant of electron beam irradiation; and 3) thin enough to transmit electron beam (<100 nm).
- TEM imaging of inorganic and biological materials has been studied well.
- Organic compounds (thin films, crystals, solids, etc.) are usually very sensitive to irradiation of electron beam (severe decomposition predominant) and rarely observed using TEM.

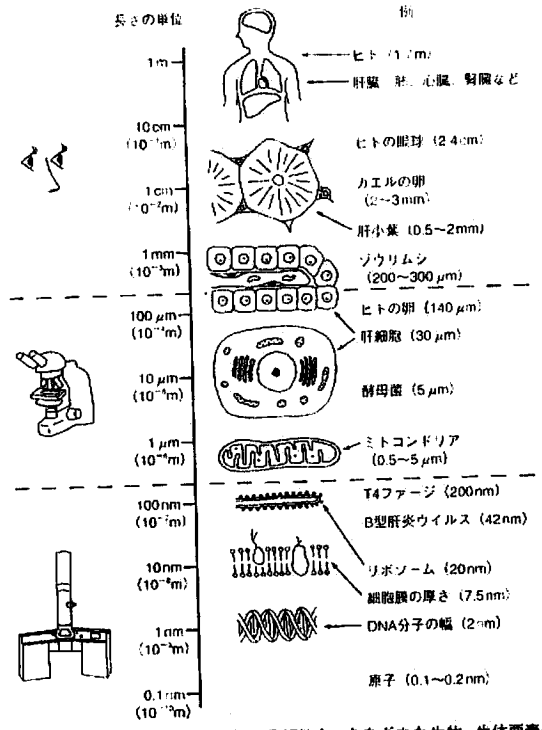

図 1.1 肉眼，光学顕微鏡，電子顕微鏡の分解能と，さまざまな生物，生体要素の大きさ

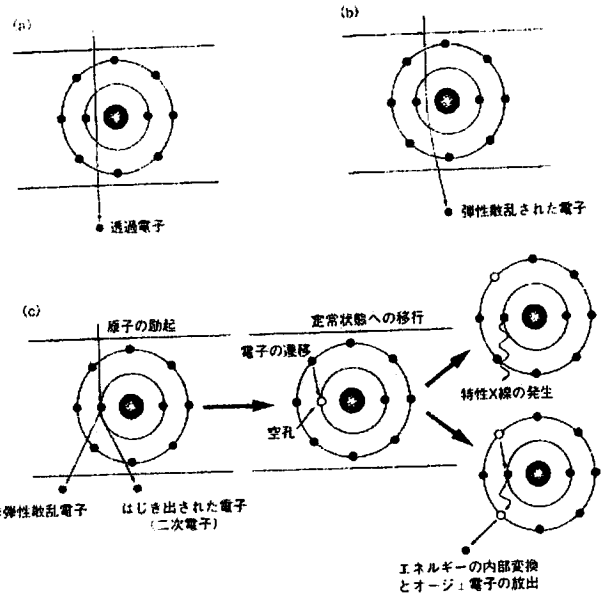

図 9.7 電子と試料の相互作用

表 6.1 光学顕微鏡と電子顕微鏡の主な構成要素

		機能				
種類	光源	波長 (nm)	鏡体内	レンズ	直接倍率	分解能	試料支持体
光学顕微鏡	電球・光線	400～500	大気圧	ガラスレンズ	×1,500	~0.2 μm	スライドグラス
電子顕微鏡	電子銃	0.0020(300 kV)	高真空	電子レンズ	×1,500,000	~0.1 nm	金属グリッド
	電子線	0.0037(100 kV)					

3.1.2 Carbon Nanotube (CNT)

- CNT is a carbon allotrope found in 1991 which consists of a central tube based on hexagon carbon frameworks and terminal half-fullerene caps.
- CNT is synthesized from carbon black or hydrocarbons with discharge, laser irradiation or metal catalysts.
- Single-wall CNT (SWNT) is often used for the purpose of TEM observation of molecules.
- Central tube region is relatively stable under chemical and electron beam irradiation conditions whereas terminal cap regions are more reactive and removable with chemical method or under thermal conditions.
- CNT has an empty hole of nanometer width inside the tube. The hole can be used for TEM analysis of single molecules as a very small "test tube".

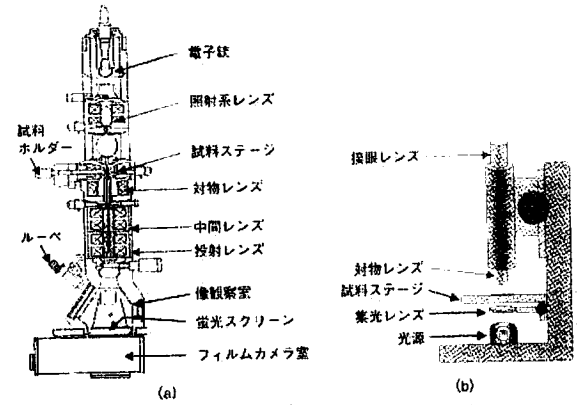

図 6.2 透過電子顕微鏡 (a) と光学顕微鏡 (b)

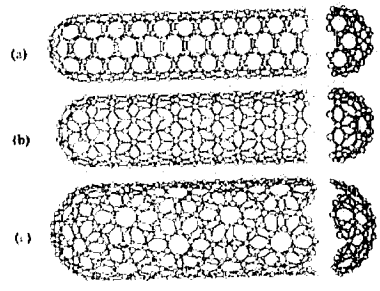

図 1.1 チューブの分類: (a) アームチェアチューブ $C_h = (5,5)$. (b) ジグザグチューブ $C_h = (9,0)$. (c) カイラルチューブ $C_h = (10,5)$。チューブの軸に対するグラファイトの六角形の向きが (a) から (c) の場合で異なる。(a) と (b) は六角形の向きが軸に対して対称的である。(c) は，螺旋対称性を持つ。チューブの終端は，フラーレンの半球 ((a) と (b) は C_{60} の半球，(c) は C_{140} の半球) で閉じている。

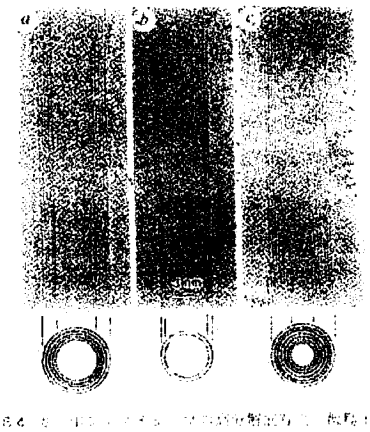

図 8.4 [illegible]

3.2 TEM Imaging of Fullerenes in CNT

References: Luzzi, D. E.; et al. *Nature* **1998**, *396*, 323;
Iijima, S.; et al. *Phys. Rev. Lett.* **2000**, *85*, 5384;
Suenaga, K.; et al. *Phys. Rev. Lett.* **2003**, *90*, 055506;
Suenaga, K.; et al. *Nano Lett.* **2004**, *4*, 2451;
Suenaga, K.; et al. *Phys. Rev. Lett.* **2006**, *96*, 088304.

3.2.1 Synthesis of Fullerenes in CNT (Peapod)

purified SWNTs (opened/ closed) —dry air, 420 °C, 20 min→ SWNTs (opened) —purified fullerene derivatives, sealed tube, high vacuum, 400–500 °C, 24–48 h→ fullerenes in SWNTs (peapod)

0.35±0.02 nm determined by TEM

- Pretreatment of SWNTs under dry air at high temperature is important to obtain high yield of peapods (80–90%) probably due to opening of the ends of SWNTs.
- Appropriate selection of diameter of SWNTs is also impotant to dope fullerenes.
- Introduction of fullerenes into SWNTs is an exothermic reaction.

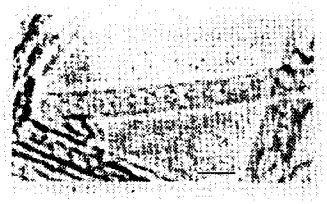

Figure 1 A single-walled carbon nanotube containing a pair of closest carbon shells concentric with the tubule axis. The diameter and centre-to-centre spacing of the internal shells are consistent with a chain of C_{60} molecules. The nanotube is surrounded by a vacuum. Scale bar, 2.0 nanometres.

表 2.2 各サイズのフラーレンを内包できる単層カーボンナノチューブの直径の最小値[2]

フラーレン	内包できるナノチューブの直径の最小値/nm
C_{60}	1.37
C_{70}	1.45
C_{78}	1.45
C_{84}	1.54

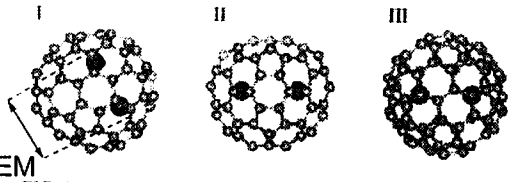

FIG. 1 (color). Three possible isomers (*I*, *II*, *III*) of $Sc_2@C_{84}$ suggested by NMR and theoretical studies (Refs. [2,3]) (C_s, C_{2v}, D_{2d}, respectively). The exact Sc atom positions were unknown except for (*III*).

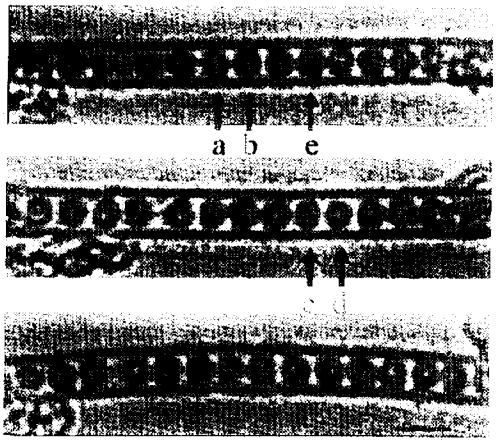

FIG. 2. HR-TEM images of the $Sc_2@C_{84}$ metallofullerenes inside SWNTs. Dark spots seen in each molecule correspond to the individual Sc atoms. Legends (a)–(e) correspond to the simulated image in Fig. 3. A JEOL 2010F electron microscope was operated at 117 keV for imaging. Bar = 2 nm.

3.2.2 Observation of Metallofullerenes in CNT

(1) TEM Image of $Sc_2@C_{84}$ in SWNT

- Position of two Sc atoms in a fullerene were successfully determined by combination of high resolution TEM imaging and simulation technique.
- The Scs were not positioned at the both side of the fullerenes. The position of Scs has not been determined by conventional NMR technique (only determination of symmetry was possible).

(2) Detection of Sc in CNT by Electron Energy-Loss Spectroscopy (EELS)

- EELS spectrum shows the energy loss of irradiated electron beam that correlates with energy levels of valence bond electrons. Therefore the spectrum contains information of each element as well as its electronic state.
- EELS showed existence of Sc atoms and the same valence state of Sc (Sc^{2+}) before and after encapsulation in SWNT.

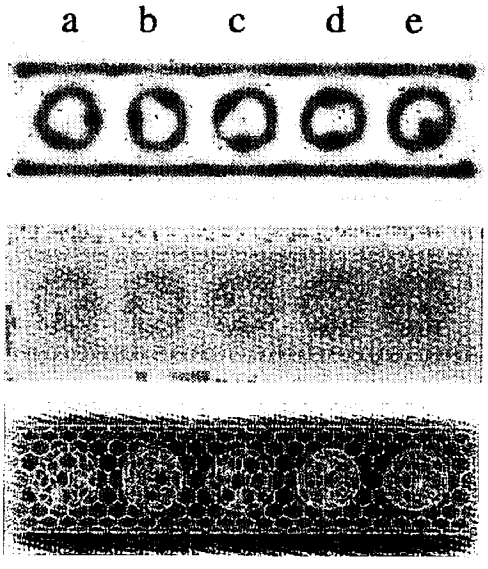

FIG. 3 (color). Simulated HR-TEM image (top panel) for various orientations of $Sc_2@C_{84}$ molecules inside SWNT. Projected atomic potential (middle panel) and models used for simulations (bottom panel) are also presented. Legends (a)–(e) correspond to those in the observed images in Fig. 2.

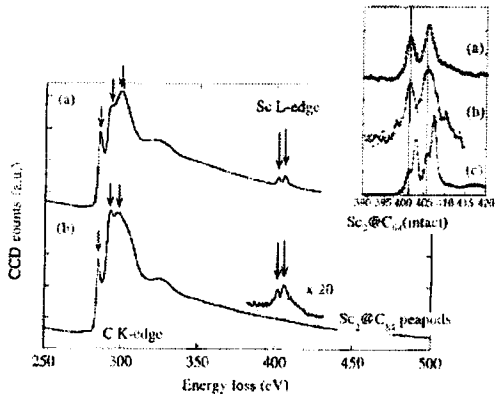

FIG. 4. EELS spectra taken from the intact $Sc_2@C_{84}$ (*a*), $Sc_2@C_{84}$ in SWNT (*b*), and Sc_2O_3 for reference (*c*). Compared with the spectrum for the Sc^{3+} in Sc_2O_3 (inset), the same valence state of the encapsulated Sc atoms (Sc^{2+}) is suggested for (*a*) and (*b*). Gatan imaging filter was used during the TEM operation for electron spectroscopy. The arrows indicate the peak positions assigned for the C *K*-edge including π^* and σ^* and the Sc L_{23}-edge.

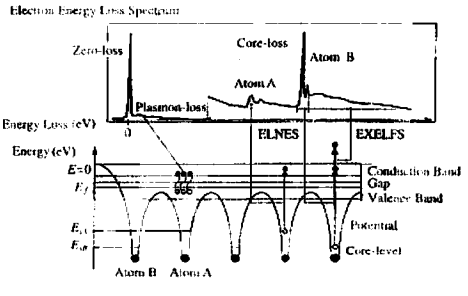

図 6.2 EELS（電子線分光）の原理図

3.2.3 Metal Atoms Transfer between Metallofullerenes in CNT

(1) Fusion and Dissociation of Defects of Fullerene in CNT

- Electron beam impact induced the defects (small holes) on the surface of fullerene. The defe... provide the holes from which imprisoned metals escape to outside of the fullerenes.
- The formation rate of the defect are estimated to be three of ten fullerenes during 5 minutes ...
- Two defects on the fullerenes coalesced to give a peanuts-like fullerene. The coalescence induces transfer of enclosed metals from one fullerene to another.

(2) Escape of a Tb Atom from $Tb_2@C_{92}$

- One Tb atom escaped from the fullerene cage through defects formed by electron beam.
- Three interactions during the "prison break" is expected: 1) Coulomb interaction of Tb^{3+} cations in the C_{92} cage; 2) ionic interaction between Tb and the C_{92} cage; and 3) interaction of Tb atoms and the defective area.

(3) Migration of Gd Atoms from $Gd@C_{82}$ to $Gd_2@C_{92}$

- One Gd atom moved to the next fullerene via the coalescence position to form Gd_3 cluster.
- Another Gd atom was transferred from right to left.
- The driving force of the Gd cluster formation might be strong interaction between the Gd atom moved and the defective area.

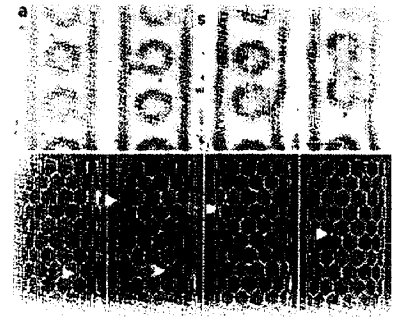

Figure 1. (a) A series of HR-TEM images for the atomic pathways opening and closing on the fullerene cage (C...). In this case all the cages were originally empty. The arrows (a) and (b) in the schematic presentations (b) indicate the formation of interlayer couplings. An atomic path, or the vacancy-type defect, is clearly seen at the fullerene cage (arrows (c) and (e)). These interlayer couplings dissociate after (arrows (a)) and (c)) and one of the paths obviously closes (arrow (e)). Then two fullerenes begin to coalesce (t = 123 s) and another kind of path is definitively induced to interconnect two adjacent fullerenes (arrow (e)). Scale bar, 1 nm.

3.2.4 Pyrrolidino-Substituted Fullerenes in CNT

- Structure and move of *N*-Me-pyrrolidino-substituted exofullerenes having no heavy metal atoms were also successfully detected.
- EELS showed electronic state change of the N atoms in SWNT. This suggests some interaction of N and CNT (probably demethylation and new bond formation).

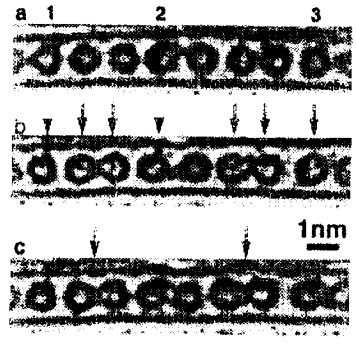

FIG. 2. A sequential HR-TEM image of $(C_{60}\text{-}C_3NH_7)_n$@SWNTs. The functional group attached to each fullerene cage is indicated by arrows and arrowheads. (a) 0 sec (b) 2 sec, and (c) 4 sec. Some of the fullerenes make rotations inside the SWNTs. Two of the adjacent fullerenes begin to fuse each other [(c)]. See also the provided movie file [10].

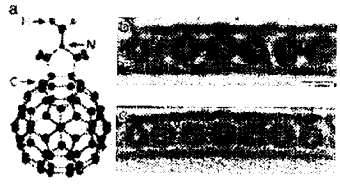

FIG. 1 (color). (a) A scheme of the used fullerene derivatives functionalized with a pyrrolidine ($C_{60}\text{-}C_3NH_7$, N-methyle-3,4-fulleropyrrolidine). HR-TEM images of a functionalized fullerene peapod (b) and (c) the nonfunctionalized fullerene peapod.

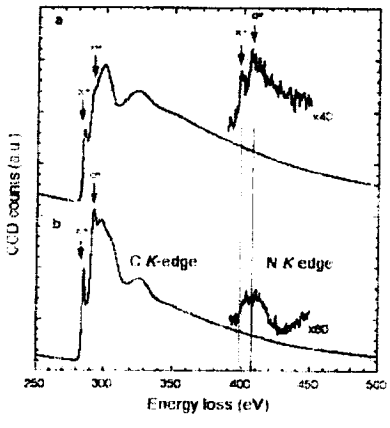

FIG. 3. (a),(b) EELS spectra taken from a crystalline particle of the fullerene derivatives ($C_{60}\text{-}C_3NH_7$) before being encapsulated and from the peapods, respectively. The fine structures of carbon represent for the fullerenes with degraded symmetry (a) and for the main contribution of SWNTs (b). The nitrogen *K* edge in (a) resembles that of nitrogen atoms in the pyrrolidine, but it completely evolves after the encapsulation in the peapod (b) because of the strong interaction with the tube wall.

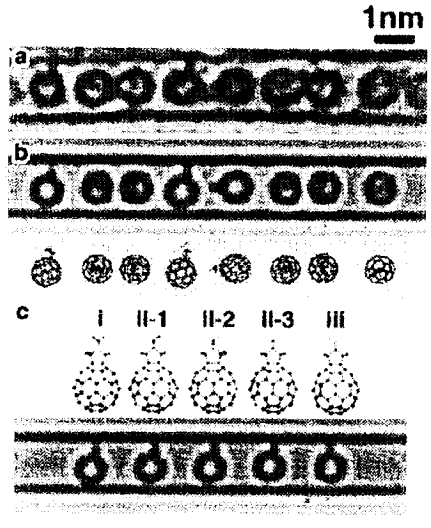

FIG. 4 (color). A comparison of the experimental HR-TEM image (a) with the simulated image (b). We have made several kinds of image simulations for the molecular structure: intact (i), with the detached hydrogen atoms (from 1–3 H atoms) (ii), or without the methyl group (iii). The latter two [(ii) and (iii)] fit reasonably well with the observed images. Note that most of the observed functional groups appearing to attach to the tube wall, suggesting the strong interaction between each functional group and the tube wall.

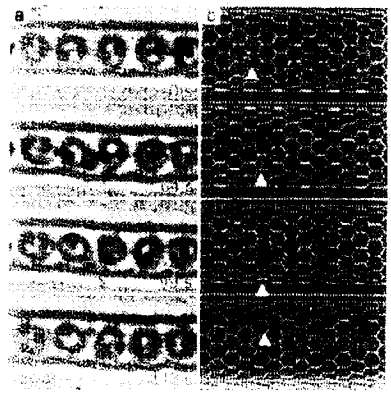

Figure 2. (a) A series of HR-TEM images showing the break out of the imprisoned Tb atoms from $Tb_2@C_{92}$ peapod. Each fullerene carries two Tb atoms at the initial stage (t = 0). One of the Tb atoms goes out through an atomic path induced between fullerene cage and tube wall (indicated by arrows). The fullerene cage undergoes a considerable deformation (t = 64 s) and the tube wall also shows some defects (t = 99 s). The escaped Tb atom wanders after inside the tube (t = 113 s). See also the provided movie file (Movie2.mov in Supporting Information) for the sequential HR-TEM images. The encapsulated Tb atoms appear in red and the migrating atom is indicated by a white arrow in the schematic presentation (b). Scale bar, 1 nm.

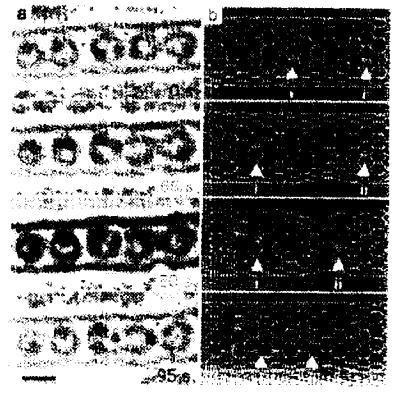

Figure 3. (a) Sequential HR-TEM images showing the migrating Gd atom from cage to cage. This SWNT is coalesced with monometallofullerenes and dimetallofullerenes ($Gd@C_{82}$ and $Gd_2@C_{92}$). The numbers of Gd atoms in each cage deduced from the initial HR-TEM image (t = 0 s) are 1, 1, 2, 2, 1 atoms (left). One of the Gd atoms in $Gd@C_{82}$ (arrow (i)) moves into the adjacent cage (t = 65 s) and a trimetallofullerene is observed (t = 80 s), followed by the migration of another Gd atom (arrow (ii)) (t = 95 s). The evolution of the number of Gd atoms in each cage is expressed as (1, 1, 2, ..., 2), (1, 1, 3, 0, 1), and finally (1, 1, 1, 1, 1) (t = 95 s). See also the provided movie file (Movie3.mov in Supporting Information) for the sequential HR-TEM images. The migrating Gd atoms are indicated by white arrows in the schematic presentation (b). Scale bar, 1 nm.

3.3 TEM Imaging of Moving Carboranes in CNT

Reference: Isobe, H.; Nakamura, E.; et al. *Science* **2007**, *316*, 853.

3.3.1 Synthesis of Carboranes **1–4** and its Encapsulation in CNT

○: BH
•: C

^{n}BuLi (1.0 equiv);
1-bromododecane (1.0 equiv)
or 1-bromodocosane (1.1 equiv)

THF
0 °C to rt, 30 min

ca. 0.8 nm

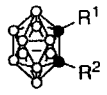

1: $R^1 = {}^nC_{12}H_{25}$-, R^2 = H (30%)
2: $R^1 = R^2 = {}^nC_{12}H_{25}$- (30%)
3: $R^1 = {}^nC_{22}H_{45}$-, R^2 = H (59%)
4: $R^1 = R^2 = {}^nC_{22}H_{45}$- (20%)

HiP_{CO} SWNT
(ø 0.9–1.2 nm)

sealed tube
2×10^{-4} Pa
160 °C, 48 h

1–4 in SWNT

• THe SWNT was oxidatively perforated with O_2 gas at 420 °C before encapsulation.

3.3.2 TEM Imaging of Encapsulated Carboranes in CNT

- Carboranes **1–4** captured in SWNTs were detected by TEM. The carborane moieties possessing high electron density were easily differenciated.
- EELS supported the presence of boron atoms in CNT.
- Comparison of contrast ratio of observed and simulated images showed the carboranes had a streched conformation.

3.3.3 TEM Imaging of Moving Carboranes in CNT

(1) Conformational Change of Carboranes

- TEM images of dynamic conformational change of carborane **4** in ca. 1.2 nm of CNT were obtained on a time scale of 2.1 seconds (0.5 sec beam irradiation + 1.6 sec aquisition of data).
- One alkyl chain did not change its position, suggesting that the alkyl chain strongly interacted with a defective area (or a hole) of CNT.
- Compared with fullerenes in CNT, the carboranes were not damaged by electron beam irradiation, probably because of their stability against electron impact.

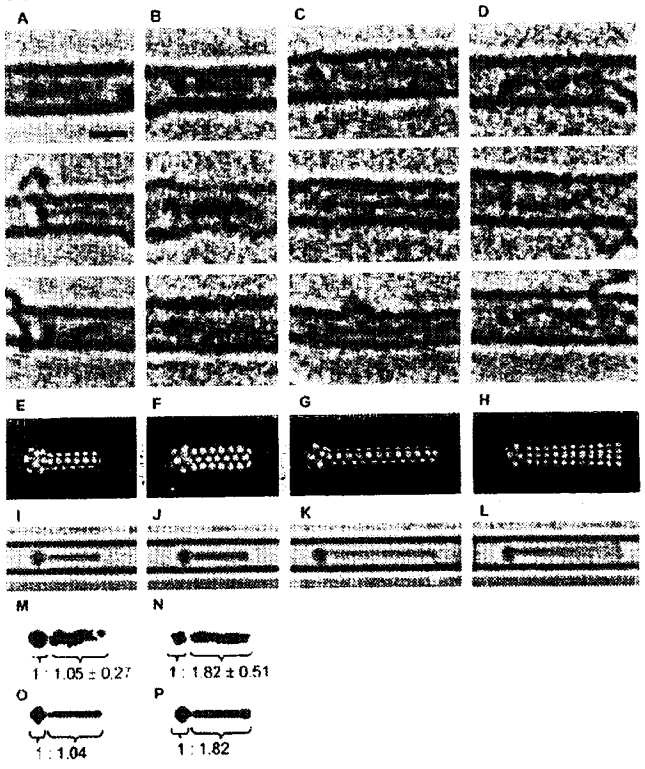

Fig. S1. Experimental TEM images of molecules 1-4 in CNTs, their models assuming a linear conformation of the side chain(s) and a narrow CNT and contrast analysis of molecules 1 and 2. (**A-D**) Three representative images of molecules 1-4, respectively. The top left picture of A is same as that shown in Fig. 1B. The scale bar shows 1 nm. (**E-H**) The corresponding molecular models in narrow CNTs (0.9 nm). This tube is too tight to house comfortably the double $C_{12}H_{25}$ and $C_{22}H_{45}$ carboranes 2 and 4. (I-L) Simulated images for the models in E-F. (**M** and **N**) Molecular images of 1 and 2 obtained by subtracting the background contrast from the top image of A and B, respectively. The values below show the image contrast ratio between the head and tail parts. (**O** and **P**) Simulated images of 1 and 2 obtained by subtracting the background contrast from images I and J, respectively.

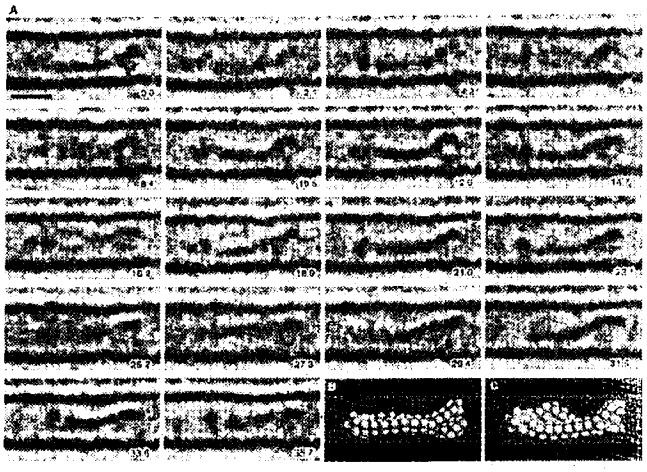

Fig. S4. TEM images of the conformational change of double $C_{22}H_{45}$ carborane **4** in a CNT of 1.2 nm diameter. The motion picture is shown in Movie S1, and the representative images are also shown in Fig. 1G. (**A**) Experimental images showing that two alkyl chains change their conformation as the molecule wobbles. The images were obtained over ca. 40 s (from top left to bottom right). The numbers at the bottom of each image show the time of the observation in seconds. The scale bar is 1 nm. (**B** and **C**) Models of the molecule in a CNT at times 4.2 s and 6.3 s, respectively. Hydrogen: white, boron: pink, carbon: gray.

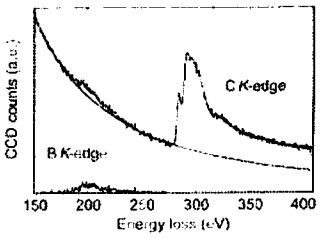

Fig. S2. EELS of double $C_{12}H_{25}$ carborane **2** in a CNT showing the presence of boron atoms. Typical EELS spectra including the boron and carbon *K*-edges at 188 eV and 284 eV in the 50 nm diameter probing area, respectively. The atomic ratio of boron to carbon was calculated to be 1.33 from a hydrogenic model, indicating that considerable numbers of carborane molecules were encapsulated in the CNT.

(2) Moving Carborane in CNT

- The carborane **2** enclosed in a CNT of 1.2 nm diameter at first moved to left (0–10.5 sec) and changed its direction to right (10.5–21 sec). The terminal of the alkyl chain then sticked to the defect on CNT to hold the carborane at one position (21–46.2 sec) before moving to far right side (46.2–58.8 sec).
- Molecular oriantation of the carborane was kept during the TEM observation.
- Sticking of the carborane to the defect may be reversible.
- Exact position of the alkyl chain and the carborane head moving too fast (>10 nm/sec) was difficult to determine under the current aquisition time (0.5 sec).

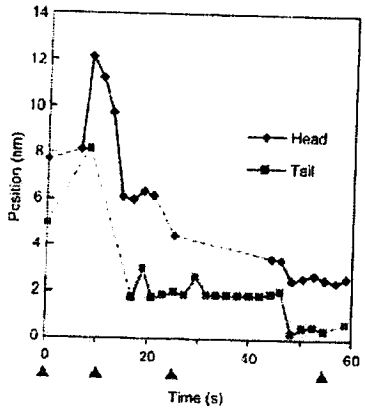

Fig. S7. Numerical analysis of the translation of double $C_{12}H_{25}$ carborane **2** through a CNT of 1.2 nm diameter. Time-dependent locations of the molecule. x-axis: time in seconds after the start of imaging (0.5 s imaging and 1.6 s read-out time intervals). y-axis: position in nm. The red triangles mark the time of the images in Fig. S6. The movie is shown in Movie S3.

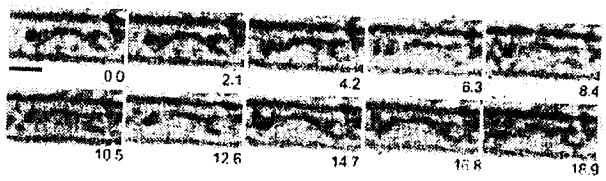

Fig. S5. Additional TEM images of the conformational change of double $C_{22}H_{45}$ carborane **4**. The motion picture is shown in Movie S2. Experimental images of a molecule different from the one discussed in the text show that the two alkyl chains change their conformation as the molecule wobbles in a CNT of 1.3 nm diameter. This molecule also appears to be attached to a defective part of the CNT wall. The images were obtained over ca. 20 s (from top left to bottom right). The numbers shown at the bottom of each image show the time of the observation in seconds. The scale bar is 1 nm.

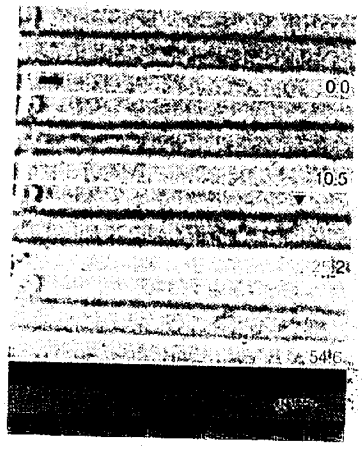

Fig. S6. Translation of double $C_{12}H_{25}$ carborane **2** through a CNT of 1.2 nm diameter without changing the orientation of the molecule. The scale bar shows 1 nm. The numbers show the time of the observation in seconds. At time 0 s, the molecule moves slowly to the left having the head toward the left, and is moving quickly at time 10.5 s (blurred image on the left). At time 25.2 s, one can see that the molecule still retains its original orientation, but the tail sticks to the upper wall. At time 54.6 s, the molecule has already moved further to the right. When the alkyl chains are seen to be very dark and visible, the two chains are overlapping at the viewing angle. The bottom panel shows a 3D model of the image at 54.6 s. See Fig. S7 for a numerical analysis of the position and Movie S3 for the motion picture over a period of ca. 60 s.

4. Summary and Prespective

4.1 Remaining Points to be Solved

4.1.1 FLS

- Applicable for light-inducing reactions only
- Clean preparation of active complex is necessary to understand the dynamics of short-lived intermediates in femtosecond order.
- A large set of molecules is required to observe spectra with sufficient S/N ratio.
- Mainly applicable for unimolecular reactions.

4.1.2 TEM Imaging

- Electronic "tags" (metals, fullerenes, carboranes, etc.) seem to be impotant to determine the position of molecules with high resolution.
- Heating under high vacuum conditions is necessary to encapsulate the molecules.
- Clean formation of encapsulated CNT that is applicable for TEM observation is difficult.
- In some cases, changes of molecules by electron beam irraditation are serious.
- Time resolution is a second order and faster reaction cannot be observed.

4.2 Application in Organic Synthesis

4.2.1 FLS

- Mechanistic study of light-induced reactions
(• Strong laser pulse-induced observation of molecular orbitals and transformation of molecules)

4.2.2 TEM Imaging

- Stractural determination of organic molecules and complexes
- Reactions in CNTs and its observation